ELSEVIER

Journal of Biomechanics 38 (2005) 467–475

JOURNAL OF BIOMECHANICS

www.elsevier.com/locate/jbiomech
www.JBiomech.com

A comparison of mechanical properties derived from multiple skeletal sites in mice

Jennifer L. Schriefer[a], Alexander G. Robling[b], Stuart J. Warden[c,d], Adam J. Fournier[a], James J. Mason[e], Charles H. Turner[c,f,*]

[a] Department of Biomedical Engineering, Purdue School of Engineering and Technology, Purdue University, Indianapolis, IN, USA
[b] Department of Anatomy and Cell Biology, Indiana University School of Medicine, Indianapolis, IN, USA
[c] Department of Orthopaedic Surgery, Indiana University School of Medicine, Indianapolis, IN, USA
[d] Centre for Health, Exercise, and Sports Medicine, School of Physiotherapy, The University of Melbourne, Melbourne, Vic, Australia
[e] Department of Aerospace and Mechanical Engineering, University of Notre Dame, Notre Dame, IN, USA
[f] Biomechanics and Biomaterials Research Center, Indiana University School of Medicine, Indianapolis, IN, USA

Accepted 26 April 2004

Abstract

Laboratory mice provide a versatile experimental model for studies of skeletal biomechanics. In order to determine the strength of the mouse skeleton, mechanical testing has been performed on a variety of bones using several procedures. Because of differences in testing methods, the data from previous studies are not comparable. The purpose of this study was to determine which long bone provides the values closest to the published material properties of bone, while also providing reliable and reproducible results. To do this, the femur, humerus, third metatarsal, radius, and tibia of both the low bone mass C57BL/6H (B6) and high bone mass C3H/HeJ (C3H) mice were mechanically tested under three-point bending. The biomechanical tests showed significant differences between the bones and between mouse strains for the five bones tested ($p<0.05$).

Computational models of the femur, metatarsal, and radius were developed to visualize the types of measurement error inherent in the three-point bending tests. The models demonstrated that measurement error arose from local deformation at the loading point, shear deformation and ring-type deformation of the cylindrical cross-section. Increasing the aspect ratio (bone length/width) improved the measurement of Young's modulus of the bone for both mouse strains ($p<0.01$). Bones with the highest aspect ratio and largest cortical thickness to radius ratio were better for bending tests since less measurement error was observed in the computational models. Of the bones tested, the radius was preferred for mechanical testing because of its high aspect ratio, minimal measurement error, and low variability.

Keywords: Biomechanical testing; Biomechanics; Osteoporosis; Three-point bending

1. Introduction

Osteoporosis is a clinical condition characterized by an increased risk of bone fracture due to decreased bone strength. To assess skeletal fragility, biomechanical measurements are used to measure the mechanical properties of the skeleton. Mechanical testing cannot be directly performed in living human subjects due to the requirement that the bone specimen be broken, so animal models afford the best means to test the skeleton's mechanical properties. Of the animal models available, the mouse is frequently used (Jamsa et al., 1998; Jepsen et al., 1997; Kodama et al., 2000; Robling and Turner, 2002; Robling et al., 2003; Shultz et al., 2003; Wergedal et al., 2002), because of the wide range of available models, including many with naturally occurring and genetically engineered diseases.

To assess the mechanical properties of the mouse skeleton and enable accurate comparisons across studies, there is a need for the standardization of

*Corresponding author. Department of Orthopaedic Surgery, Room 600, 541 Clinical Drive, Indiana University School of Medicine, Indianapolis, IN 46202, USA. Tel.: +1-317-274-3226; fax: +1-317-274-3702.
E-mail address: turnerch@iupui.edu (C.H. Turner).

0021-9290/$ - see front matter © 2004 Elsevier Ltd. All rights reserved.
doi:10.1016/j.jbiomech.2004.04.020

mechanical testing procedures. Currently, no such standardization exists; previous studies use a variety of techniques and skeletal sites. Techniques have included compressive (Ito et al., 2002), tensile (Bini et al., 2002), torsional (Brodt et al., 1999; Lind et al., 2001), four-point bending (Brodt et al., 1999; Jepsen et al., 2001; Smith et al., 2000) and three-point bending (Jamsa et al., 1998; Robling and Turner, 2002; Wergedal et al., 2002) tests. Of these, three-point bending is a simple, reproducible test, making it the preferred method of mechanical testing in small animals (Jamsa et al., 1998; Turner and Burr, 1993).

Bones come in different shapes and sizes, and none have the geometry and gross morphology of an ideal mechanical test specimen. It is not clear which bone is best to use for determining the mechanical properties of the mouse skeleton during three-point bending. Many bones have previously been used, including the femur (Jamsa et al., 1998; Jepsen et al., 1997; Kodama et al., 2000; Wergedal et al., 2002), humerus (Lind et al., 2001), metatarsal (Li et al., 1991), radius (Robling and Turner, 2002), and tibia (Jamsa et al., 1998; Kodama et al., 2000). These different skeletal sites have produced large variations in the calculated bone material properties. However, much of this site-specific variation is probably artifact based upon the fact that some bones have a less favorable geometry for a bending test. A preferable bone for bending tests is one that has a large length to width ratio and a consistent cross-sectional shape along its entire length. In order to calculate the correct bone tissue properties from a bending test, the bone's aspect ratio (the ratio of the length to width) should be over twenty (Spatz et al., 1996). If the bone is short and stout the bending test will generate a larger shear deformation in addition to bending deformation thus reducing the value of Young's modulus derived from the test. Hence a bone that best resembles a long, narrow tube and therefore has a large aspect ratio makes the better test specimen.

This study aimed to determine the most favorable long bone for assessing the mechanical properties of the mouse skeleton in three-point bending. Assessment was based upon which bone provided the (1) largest aspect ratio with a constant cross-section, (2) most accurate value for the Young's modulus of mouse bone, which has been determined from ultrasonic measurements (Kohles et al., 1997; Somerville et al., 2004) and nanoindentation measurements (Akhter et al., 2002), and (3) produced the most precise (reproducible) test results. We also evaluated the error inherent in the three-point bending tests based on the bone's geometry using computational models. Five candidate bones were investigated, the femur, humerus, third metatarsal, radius, and tibia, from both the high bone mass C3H/HeJ (C3H) and low bone mass C57BL/6H (B6) strains of mice. We hypothesized those bones with the highest aspect ratio, such as the radius, would yield the most accurate and precise material properties from three-point bending tests. We defined accuracy of the results as material properties that approach published values from tissue-level (i.e. ultrasonic and nanoindentation) tests, and precise results as those with the least amount of variance.

2. Methods

Thirteen virgin female C57BL/6H (B6) and 12 virgin female C3H/HeJ (C3H) mice were purchased from Harlan Inc. (Indianapolis, IN) and Jackson Laboratory (Bar Harbor, ME), respectively. These two strains of mice were chosen for their very different biomechanical properties (Turner et al., 2000; Robling and Turner, 2002; Wergedal et al., 2002). Animals were housed at Indiana University's Laboratory Animal Resource Center and all procedures performed were in accordance with the Institutional Animal Care and Use Committee's guidelines. At 20 weeks of age, the animals were sacrificed by cervical dislocation under isoflurane-induced anesthesia and the left femur, humerus, third metatarsal, radius, and tibia were dissected free, cleaned of soft tissue, and stored in 70% alcohol for 3 months prior to testing. Short-term storage in 70% alcohol has been shown to have no negative effects on the mechanical properties of bone (Linde and Sorensen, 1993).

2.1. Bone geometry

To calculate material properties from tests of whole bones, the cross-sectional geometry at the failure site is necessary. Bone geometry was determined from a midsection slice of each bone scanned using a desktop μCT with a 7 μm voxel size (μCT 20; Scanco Medical AG, Bassersdorf, Switzerland). The scanned images were rotated so that the mediolateral axis coincided with the x-axis (Fig. 1A) and imported into Scion Image v4.0.2 for Windows (Scion Corp., Frederick, MD) in which the second moment of area about the mediolateral axis (I_X; mm^4) and the maximum diameter of the section in the anterior–posterior plane (d; mm) were calculated using standard and customized macros. The neutral bending axis is defined as the axis through the center of mass of the section in the mediolateral plane.

2.2. Mechanical properties

The bones were loaded to failure by three-point bending. Prior to testing they were rehydrated overnight in 0.9% NaCl at room temperature. Testing was performed on a miniature materials testing machine (Vitrodyne V1000; Liveco, Inc., Burlington, VT, USA),

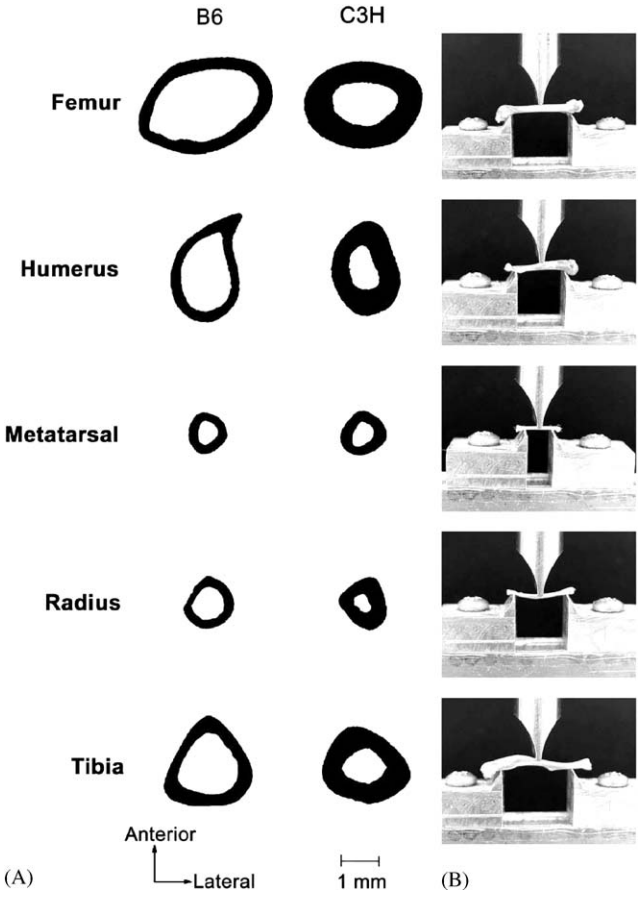

Fig. 1. (A) Representative μCT cross-sectional images of each bone from both the B6 and C3H strains. The bones were scanned through the midshaft, which was also the site at which failure occurred during three-point bending. Note the increased cortical thickness in the C3H bones. (B) Representative photographs of mechanical testing of each bone. The span between the two lower supports was set at the largest possible distance without compromising the stability of the bone.

which has a force resolution of 0.05 N. The lower supports were set at the maximal allowable distance for each bone without compromising the test. The support distances were as follows: 10.0 mm for the femur, 7.5 mm for the humerus, 4.5 mm for the third metatarsal, 8.4 mm for the radius, and 11.2 mm for the tibia (Fig. 1B). The crosshead speed during testing was 0.2 mm/s, and force-displacement data was collected every 0.01 s. From the data, a force versus displacement graph was created and the ultimate force (F_U; N), yield force (F_Y; N), stiffness (S; N/mm), and postyield energy to failure (U_{PY}; mJ) were calculated (Fig. 2). The yield point was defined using a 0.015 mm offset parallel to the stiffness.

2.3. Material properties

Combining the geometric calculations and the biomechanical test results, the material properties of each

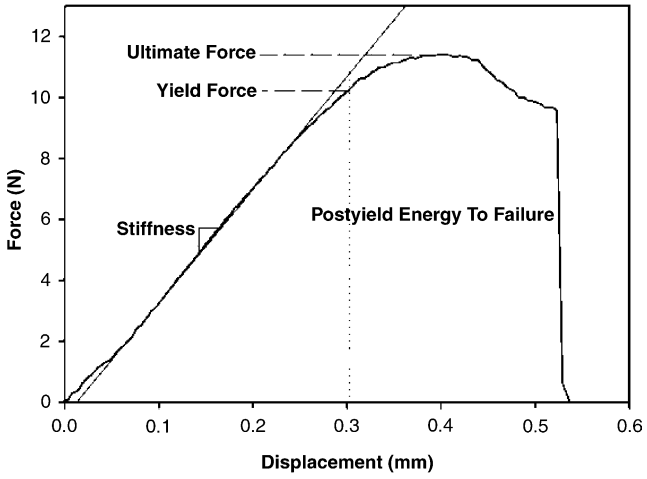

Fig. 2. Representative force–displacement graph generated from a tibia three-point bending test. Mechanical properties derived from this graph included ultimate force (peak of the curve on the y-axis), yield force (defined using a 0.015 mm offset parallel to the stiffness), stiffness (slope of the linear portion of the curve) and postyield energy to failure (area under the curve after the yield point).

bone were calculated as follows:

$$\sigma_U = F_U\left(\frac{Lc}{4I_x}\right) \quad E = \frac{F}{D}\frac{L^3}{48I_x} \quad u = U\frac{3D^2}{4I_xL}$$

$$\varepsilon_{PY} = \frac{6D_{PY}d}{L^2}, \tag{1}$$

where σ_U is the ultimate stress (MPa), L is the span of the lower supports (mm), c is one half of the bone diameter measured perpendicular to the neutral axis (mm), E is Young's modulus (GPa), D is the displacement (mm), u is the modulus of toughness (MPa), U is energy to failure (mJ), ε_{PY} is the postyield strain, and D_{PY} is the displacement after the yield point (mm).

The aspect ratio was defined as:

$$\text{Aspect ratio} = \frac{L}{d}, \tag{2}$$

where d is the diameter at the midshaft.

2.4. Evaluation of error

Three-point bending of a tubular bone induces at least three sources of measurement error. First, there is shearing displacement in the bone that adds to the measured displacement. Second, there is local deformation where the loader contacts the bone. Finally, the loading force causes a ring-type deformation of the hollow bone's cross-section.

The error due to shearing displacement was calculated using Timoshenko's correction factors with the equation for Young's Modulus:

$$E_T = \frac{F}{D}\frac{L^3}{48I_x}\left(1 + 12\left(\frac{E}{G}\right)k\frac{I_x/A}{L^2}\right), \tag{3}$$

where E_T is the Young's modulus using Timoshenko's correction factors, k is a constant equal to 1.2, G is the shear modulus, and A is the cross-sectional area (Gere and Timoshenko, 1984). The shear modulus was assumed to be 6.0, based on published values from ultrasonic measurements (Kohles et al., 1997). The Young's modulus with Timoshenko's correction factors were only applied to the femur, metatarsal, and radius because these bones had fairly consistent cross-sectional shapes along their length. The other two bones tested, the tibia and humerus, varied considerably in cross-sectional shape and therefore did not fit the criteria of the Timoshenko calculation.

Errors due to local deformation of the specimen or ring deformation were estimated using finite element analysis. A three-dimensional, orthotropic linear finite element model of the B6 and C3H femur, metatarsal, and radius was created using ANSYS 6.1 (Ansys, Inc., Canonsburg, PA). Models of the humerus and tibia were not created because these bones have a large variance in their cross-sectional shape longitudinally, so they could not be approximated as a cylinder. Bones were modeled as orthotropic cylinders having a diameter and cortical thickness as measured from the μCT images, and a length equal to the span between the experimental mechanical testing supports. The following material properties were used: $E_{11} = 13.94\,\text{GPa}$, $E_{22} = 14.3\,\text{GPa}$, $E_{33} = 19.1\,\text{GPa}$, $G_{12} = 5.8\,\text{GPa}$, $G_{23} = 6.7\,\text{GPa}$, $G_{31} = 6.0\,\text{GPa}$, and $\upsilon = 0.35$ (Kohles et al., 1997). The element type chosen was a 20 noded cube having mid-nodes along each side to allow for modeling of curved edges. A volumetric sweep was applied to construct an equally spaced mesh. Each model was subjected to three-point bending with a defined preyield displacement, and the reaction force output was calculated. Young's modulus was estimated from the force and displacement values. Additional models with varied aspect ratios or cortical thickness to radius ratios were created to determine the effect of each of these parameters on the error of the tests.

2.5. Statistical methods

Differences between the bones of both the C3H and B6 mouse strains were tested for significance using a two-way analysis of variance (ANOVA) with repeated measures. Significant interaction was found between the bone and strain for each measure tested, so Tukey–Kramer post-hoc tests were performed for all pairwise comparisons. Variability within the measurements of the material properties was determined by calculating the coefficient of variation as standard deviation divided by the mean (reported as percent of mean). To test the slope of the Young's modulus versus aspect ratio, regression analyses were used for each mouse strain. All tests were two-tailed with a level of significance set at 0.05.

3. Results

There were significant differences between the two strains of mice in ultimate force (F_U), yield force (F_Y), stiffness (S), and postyield energy to failure (U_{PY}) (Fig. 3). Similarly, the material properties of ultimate stress (σ_U), Young's modulus (E), modulus of toughness (u), and postyield strain (ε_{PY}) were significantly different between mouse strains (Fig. 4). Significant interaction was found between the strain and the bone tested for each material property calculated.

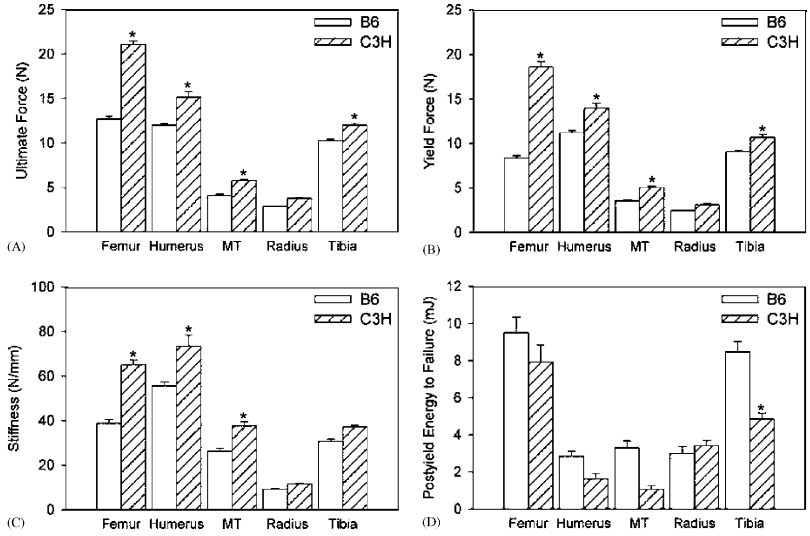

Fig. 3. (A) Ultimate force, (B) yield force, (C) stiffness, and (D) postyield energy to failure in each of the bones and mouse strains. *Indicates significant difference between B6 and C3H strains ($p<0.05$). Error bars represent ± 1 SE.

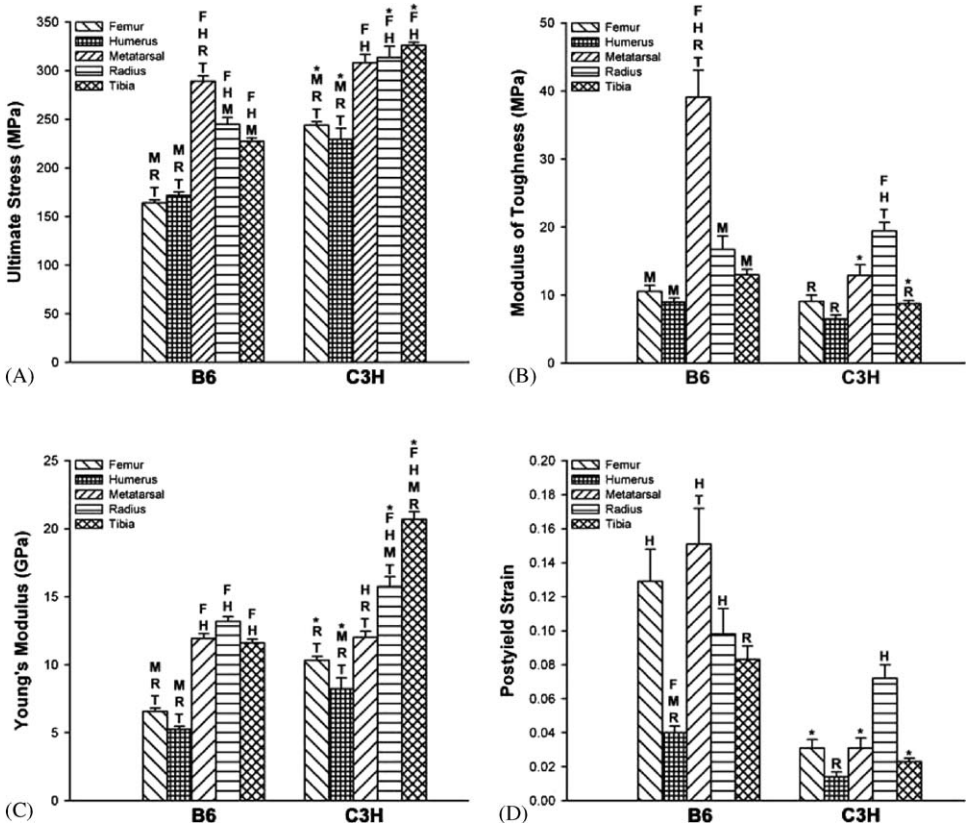

Fig. 4. (A) Ultimate stress, (B) modulus of toughness, (C) Young's modulus, and (D) postyield strain in each of the bones and mouse strains. The letters above the bars indicate significant difference ($p<0.05$) between the bone represented by the bar and the bone represented by the letter (F = femur, H = humerus, M = metatarsal, R = radius, T = tibia) within the strain. *Indicates significant difference between B6 and C3H strains ($p<0.05$). Error bars represent ± 1 SE.

Material properties differed significantly among bones in each strain (Fig. 4). The radius and tibia consistently had high values for all material properties examined, while the humerus possessed the lowest values. The material properties were positively associated with the aspect ratio of each bone. Specifically, a positive association was found between the aspect ratio and Young's modulus in both strains of mice (B6: $r^2 = 0.67$, $p<0.01$; C3H: $r^2 = 0.65$, $p<0.01$) (Fig. 5). In both strains, the radius had the largest aspect ratio followed by the tibia, while the humerus had the lowest.

The tests displayed variable reproducibility for measures of Young's modulus, ultimate stress, and modulus of toughness (Fig. 6). The tibia was consistently on the low end of the CV range for both mouse strains, whereas the femur and radius fell generally midrange. Tests of the humerus and metatarsal were generally the least consistent.

The measurement errors associated with three-point bending were calculated using finite element models. When a solid cylinder with an aspect ratio of 5 was tested in three-point bending, the value obtained for Young's modulus was 29% below the expected value of 19.1 GPa (Fig. 7A). However, when an aspect ratio of 10 was used Young's modulus was only 4% below the expected value. The cortical thickness had to be at least 33% of the radius for the measured value of Young's modulus to fall within 95% of the expected value (Fig. 7B). If the bone had a thin cortical thickness (<33% of its radius), ring-type deformation was observed. The

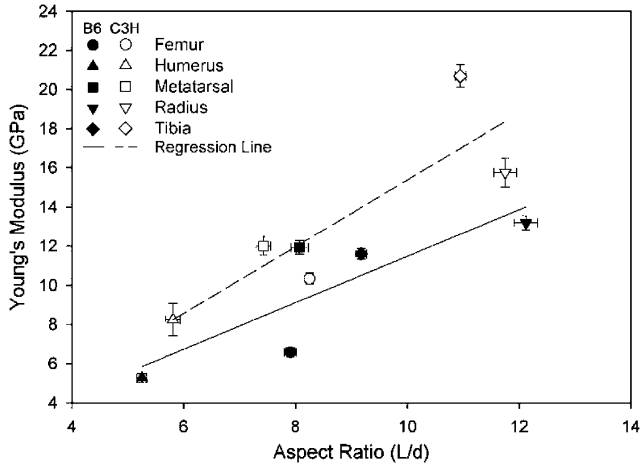

Fig. 5. Aspect ratio versus Young's modulus. The lines of regression for both the B6 and C3H mouse strains were significantly correlated ($p<0.05$). Error bars represent ± 1 SE.

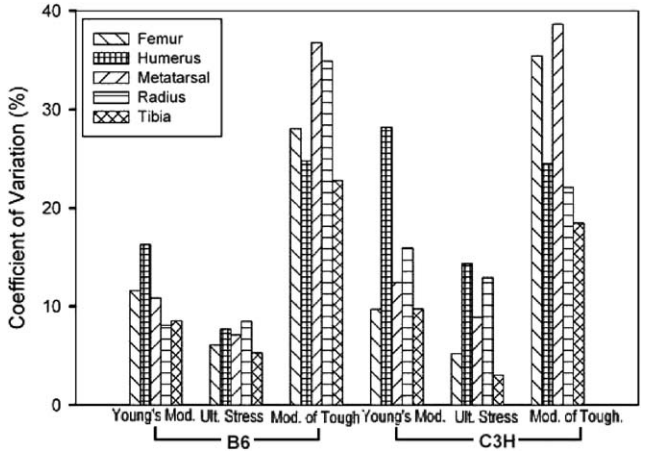

Fig. 6. Coefficient of variation of Young's modulus, ultimate stress, and the modulus of toughness in both mouse strains.

estimated error between the models' output and the material properties assigned to the model was 5.3% and 8.3% for the C3H and B6 radii, respectively (Table 1 However, the error for the C3H and B6 femurs was 12.5% and 24.7%, respectively, and 23.8 and 21.9% for the C3H and B6 metatarsals.

4. Discussion

Our objective was to determine which long bone of the mouse skeleton was the most favorable to use when assessing the mechanical properties, considering both the accuracy and consistency of the test results. We found that the radius was a good bone to test because its superior aspect ratio led to material properties that were closest to the previously published properties of bone in both strains, although the tests showed some variability. The radius also had a round and long, straight morphology, which satisfies the beam criteria more fully than other bones tested, and it had the least amount of measurement error as determined by the computational models. The humerus was the least favorable bone to test because its low aspect ratio led to material properties far from the published properties of bone and it had high variability with a nonprismatic cross-sectional shape.

During three-point bending, the main component of the deflection of bone is bending, although local deformation, ring-type and shear displacement also occur. The ratio of bending and shear contributions is dependent on the aspect ratio, as the aspect ratio is inversely proportional to the shear component (Spatz et al., 1996). Our results support the positive correlation between aspect ratio and the calculated Young's modulus described by Spatz et al. (1996). In order to minimize the shear component and promote a pure bending test, the aspect ratio should be maximized.

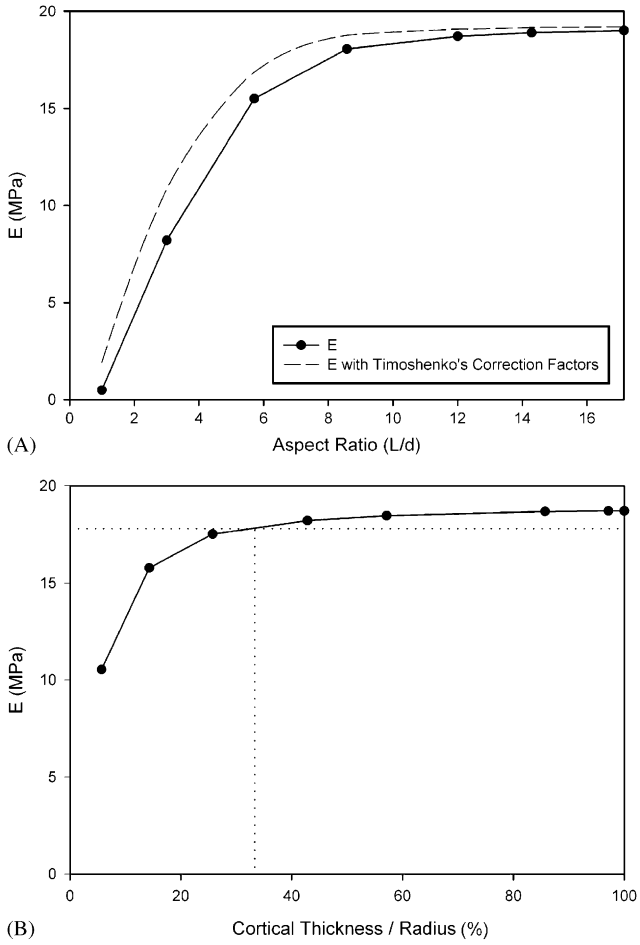

Fig. 7. (A) Effect of aspect ratio on a solid cylinder as determined by finite element models. The solid line represents the values of Young's modulus predicted by the model and the dashed line represents the Young's modulus after Timoshenko's correction factors have been applied. A difference exists between the two lines due to the sources of error other than shear deformation inherent in the tests. The Young's modulus remains within 95% of the predicted value of 19.1 GPa until the aspect ratio falls below 8.5. (B) Effect of cortical thickness to radius ratio based on the computational model. The experimental modulus is within 95% of the predicted modulus until the cortical thickness is less than 33% of the radius.

Once the aspect ratio is large the shear forces are minimal and the material properties are not directly influenced by the aspect ratio. When testing mouse bones the span between supports should be increased as much as the bone allows. The increased aspect ratio will then yield values for the calculated Young's modulus in mouse bone that are closer to the published values ranging from 19.1 to 30.5 GPa in mice and rats using ultrasonic and nanoindentation techniques (Akhter et al., 2002; Kohles et al., 1997; Somerville et al., 2004). Due in part to small aspect ratios, the results of Young's modulus in whole bones during three-point bending tests tend to be far less than the published value (Akhter et al., 2000; Jamsa et al., 1998; Robling and

Table 1
Estimation of error from the computational models

Bone	Aspect ratio (L/d)	Ct. Th./radius (%)	Measured E (MPa)	Error (%)	Corrected E (MPa)
Femur					
B6	7.9	18.9	6.6±0.2	34.7	10.1±0.4
C3H	8.3	41.3	10.3±0.3	12.5	11.8±0.3
Metatarsal					
B6	7.5	30.0	12.0±0.4	21.9	15.4±0.5
C3H	6.8	30.3	12.0±0.5	23.8	15.7±0.6
Radius					
B6	12.0	25.7	13.2±0.4	8.3	14.4±0.4
C3H	11.7	41.7	15.7±0.7	5.3	16.6±0.8

Values are mean ±SE.

Turner, 2002). However, maximizing the aspect ratio will help to resolve this problem.

A large aspect ratio is difficult to achieve using whole bones because the bones are not long enough in relation to their width, but we attempted to maximize the aspect ratio in our tests by moving the supports as far as possible without compromising the stability of the bone. Published reports of femoral tests have used a distance as small as 2 mm between the supports (Li et al., 2002), whereas we used 10 mm in this study. This large variation in the distance between supports and, consequently, aspect ratio, leads to inconsistency between results. Akhter et al. (2000) found an ultimate stress and Young's modulus of nearly half that reported in this study in femurs from the B6 and C3H mice, but they used a span between the lower supports of 5 mm. The differences in the values of the material properties can be attributed to testing error from using a smaller span between the test supports, and therefore imposing a smaller aspect ratio. In this study, the shape of the radius afforded the highest aspect ratio of the long bones tested.

Another contributor to the discrepancy between measured and predicted values of Young's modulus during testing is the ring-type deformation that occurs when the cortical thickness of the bone is small. A bone with a thin cortical shell loses its circular shape during testing and deforms into an oval (Fig. 8) as observed in the computational model. This deformation is most significant when the cortical thickness is less than 33% of the bone's radius, which occurs with all of the B6 bones, and is most significant with the B6 femur. When ring deformation occurs, displacement is measured that is not due to bending, resulting in another source of error that changes the measured value of Young's modulus.

The measured Young's modulus was significantly below the published values due in part to displacement from shear, local, and ring-type deformation. To measure this error, computational models were created using a finite element software package. The shear contribution of Young's modulus was examined by applying Timoshenko's correction factors. With the correction factors applied, the measured values of Young's modulus were closer to reported values from tissue-level tests, but were still significantly lower. These results suggest that the tissue-level tests might overestimate the value of Young's modulus in a whole bone. Alternatively, there could be other sources of experimental error in a three-point bending test other than those examined in this study.

The computational models were able to provide an error estimate between the measured Young's modulus and the published properties of bone. These models showed that the amount of error not due to bending in the radius was less than 10% while in the B6 femur it was as high as 35% (Table 1), suggesting that the least amount of error is associated with bones that have a large aspect ratio and large cortical thickness.

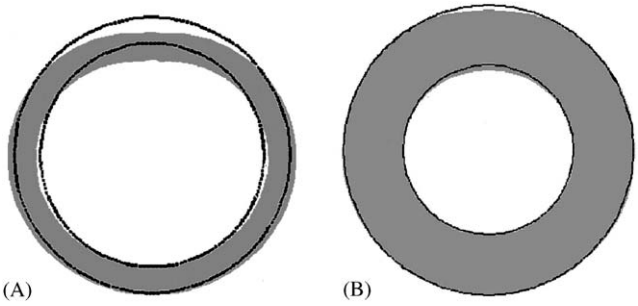

Fig. 8. Representative images from the computational model of the (A) B6 femur and (B) C3H femur before and after three-point bending. The dotted lines outline the shape of the bone prior to testing. The cortical thicknesses used were 0.12 and 0.25 mm for the B6 and C3H femur, respectively, which were average values measured from the test specimens. The B6 bone displays significantly more ring deformation than the C3H bone, which nearly maintains its circular shape after bending.

It is also possible that the different bones of the mouse skeleton have slightly different values of Young's moduli. However, besides the Young's modulus of the C3H tibia, none of the bones had a Young's moduli close to the values reported in the literature for the femur and tibia, so the variance in Young's modulus between bones cannot be the only explanation for the discrepancy between measured and published values.

An important outcome to consider when determining the most suitable bone for mechanical testing is reproducibility of tests. The coefficient of variation was very high for tests using the third metatarsal. Because this bone is very small it is difficult to position it properly and consistently, most likely causing the large coefficient of variation. Although the metatarsal met the criteria of being straight and round with a constant cross-sectional geometry, its small size makes it a very difficult bone to test with a high level of precision.

In contrast, the tibia had the lowest coefficient of variation, which could be due to the shape of tibia allowing ease of positioning during testing. The tibia is a large bone with a flat side that rested on the support, allowing the tibia to be positioned in exactly the same manner during each test. Although the more triangular cross-sectional shape of the tibia made it a less attractive bone for testing in terms of the Euler–Bernoulli beam theory, this feature contributed to the high reproducibility of the test. The low coefficient of variation for the tibia has been reported previously when performing mechanical testing (Jamsa et al., 1998). Therefore, in order to minimize variation in a study, a bone that can be simply positioned in a repeatable manner should be chosen.

The tibia produced precise results because the morphology of the bone allowed it to be easily positioned, but the continually changing cross-sectional geometry makes it an inaccurate bone to test. The results of our tests for the tibia were very close to published values of Young's modulus for the C3H bones, however, if the exact midshaft of the bone is not scanned or broken, the results could be very different due to its large variance in cross-sectional area. The Young's modulus of the C3H tibia was nearly double that of the B6 tibia, which demonstrates some of the variability of the bone. Therefore, the tibia can be a precise bone to test, but caution should be used because its cross-sectional and longitudinal morphology does not lend itself to accurate results.

As expected, the C3H bones were stronger and more brittle than the B6 bones, shown by increased ultimate stress and decreased postyield strain. The increased ultimate stress and Young's modulus in C3H bones was also reported by Turner et al. (2000) and Akhter et al. (2000). This increased strength may be attributed to an increased volumetric bone mineral density in the C3H bones. The bones from C3H mice are more brittle probably because of higher mineral content in cortical bone of C3H mice (Turner et al., 2000).

In conclusion, when assessing the strength of the skeleton, maximizing the aspect ratio of the test specimen is important for producing the most accurate results. Based on its consistently round shape, high aspect ratio, more accurate value for calculated Young's modulus, and lowest error values as computed by the finite element model, the radius is the preferred bone to use in three-point bending tests.

Acknowledgements

The work was supported by a grant from the National Institutes of Health (AR046530). Dr. S.J. Warden is supported by a National Health and Medical Research Council (Australia) CJ Martin Fellowship (reg key 209169).

References

Akhter, M.P., Iwaniec, U.T., Covey, M.A., Cullen, D.M., Kimmel, D.B., Recker, R.R., 2000. Genetic variations in bone density, histomorphometry, and strength in mice. Calcified Tissue International 67, 337–344.

Akhter, M., Roy, M., Rho, J., 2002. Breed-related variation of cortical bone intrinsic mechanical properties. Transactions of the Orthopaedic Research Society 27, 0566.

Bini, F., Marinozzi, A., Marinozzi, F., Patane, F., 2002. Microtensile measurements of single trabeculae stiffness in human femur. Journal of Biomechanics 35, 1515–1519.

Brodt, M.D., Ellis, C.B., Silva, M.J., 1999. Growing C57Bl/6 mice increase whole bone mechanical properties by increasing geometric and material properties. Journal of Bone and Mineral Research 14, 2159–2166.

Gere, J.M., Timoshenko, S.P., 1984. Mechanics of Materials. PWS-Kent, Boston.

Ito, M., Nishida, A., Koga, A., Ikeda, S., Shiraishi, A., Uetani, M., Hayashi, K., Nakamura, T., 2002. Contribution of trabecular and cortical components to the mechanical properties of bone and their regulating parameters. Bone 31, 351–358.

Jamsa, T., Jalovaara, P., Peng, Z., Vaananen, H.K., Tuukkanen, J., 1998. Comparison of three-point bending test and peripheral quantitative computed tomography analysis in the evaluation of the strength of mouse femur and tibia. Bone 23, 155–161.

Jepsen, K.J., Schaffler, M.B., Kuhn, J.L., Goulet, R.W., Bonadio, J., Goldstein, S.A., 1997. Type I collagen mutation alters the strength and fatigue behavior of mov13 cortical tissue. Journal of Biomechanics 30, 1141–1147.

Jepsen, K.J., Pennington, D.E., Lee, Y.L., Warman, M., Nadeau, J., 2001. Bone brittleness varies with genetic background in A/J and C57BL/6J inbred mice. Journal of Bone and Mineral Research 16, 1854–1862.

Kodama, Y., Umemura, Y., Nagasawa, S., Beamer, W.G., Donahue, L.R., Rosen, C.R., Baylink, D.J., Farley, J.R., 2000. Exercise and mechanical loading increase periosteal bone formation and whole bone strength in C57BL/6J mice but not in C3H/Hej mice. Calcified Tissue International 66, 298–306.

Kohles, S.S., Bowers, J.R., Vailas, A.C., Vanderby, R., 1997. Ultrasonic wave velocity measurement in small polymeric and

cortical bone specimens. Journal of Biomechanical Engineering 119, 232–236.

Li, K.C., Zernicke, R.F., Bernard, R.J., Li, A.F., 1991. Differential response of rat limb bones to strenuous exercise. Journal of Applied Physiology 70, 554–560.

Li, X., Masinde, G., Gu, W., Wergedal, J., Mohan, S., Baylink, D.J., 2002. Genetic dissection of femur breaking strength in a large population (MRL/MpJ × SJL/J) of F2 mice: single QTL effects, epistasis and pleiotropy. Genomics 79, 734–740.

Lind, P.M., Lind, L., Larsson, S., Orberg, J., 2001. Torsional testing and peripheral quantitative computed tomography in rat humerus. Bone 29, 265–270.

Linde, F., Sorensen, H.C., 1993. The effect of different storage methods on the mechanical properties of trabecular bone. Journal of Biomechanics 26, 1249–1252.

Robling, A.G., Turner, C.H., 2002. Mechanotransduction in bone: genetic effects on mechanosensitivity in mice. Bone 31, 562–569.

Robling, A.G., Li, J., Shultz, K.L., Beamer, W.G., Turner, C.H., 2003. Evidence for a skeletal mechanosensitivity gene on mouse chromosome 4. The FASEB Journal 17, 324–326.

Shultz, K.L., Donahue, L.R., Bouxsein, M.L., Baylink, D.J., Rosen, C.J., Beamer, W.G., 2003. Congenic strains of mice for verification and genetic decomposition of quantitative trait loci for femoral bone mineral density. Journal of Bone and Mineral Research 18, 175–185.

Smith, E.A., Frankenburg, E.P., Goldstein, S.A., Koshizuka, K., Elstner, E., Said, J., Kubota, T., Uskokovic, M., Koeffler, H.P., 2000. Effects of long-term administration of vitamin D_3 analogs to mice. Journal of Endocrinology 165, 163–172.

Somerville, J.M., Aspden, R.M., Armour, K.E., Armour, K.J., Reid, D.M., 2004. Growth of C57Bl/6 mice and the material and mechanical properties of cortical bone from the tibia. Calcified Tissue International 74, 469–475.

Spatz, H.-C., O'Leary, E.J., Vincent, J.F.V., 1996. Young's moduli and shear moduli in cortical bone. Proceedings of the Royal Society of London, Series B; Biological Sciences 263, 287–294.

Turner, C.H., Burr, D.B., 1993. Basic biomechanical measurements of bone: a tutorial. Bone 14, 595–608.

Turner, C.H., Hsieh, Y.-F., Müller, R., Bouxsein, M.L., Baylink, D.J., Rosen, C.J., Grynpas, M.D., Donahue, L.R., Beamer, W.G., 2000. Genetic regulation of cortical and trabecular bone strength and microstructure in inbred strains of mice. Journal of Bone and Mineral Research 15, 1126–1131.

Wergedal, J.E., Sheng, M.H.-C., Ackert-Bicknell, C.L., Beamer, W.G., Baylink, D.J., 2002. Mouse genetic model for bone strength and size phenotypes: NZB/B1NJ and RF/J inbred strains. Bone 31, 670–674.